Article

Chinese Science Bulletin

Geography

March 2012 Vol.57 No.9: 1046–1054
doi: 10.1007/s11434-011-4933-x

Modeling the radiation balance of different urban underlying surfaces

CUI YaoPing[1,2], LIU JiYuan[1], HU YunFeng[1], WANG JunBang[1] & KUANG WenHui[1*]

[1] *Institute of Geographic Sciences and Natural Resources Research, Chinese Academy of Sciences, Beijing 100101, China;*
[2] *Graduate University of Chinese Academy of Sciences, Beijing 100049, China*

Received August 24, 2011; accepted December 6, 2011; published online January 31, 2012

An urban net all-wave radiation parameterization scheme is evaluated using annual datasets for 2010 recorded at a Beijing urban observation site. The statistical relationship between observed data and simulation data of net radiation has a correlation coefficient of 0.98 and model efficiency of 0.93. Therefore, it can be used to simulate the radiation balance of Beijing. This study analyzes the variation in the radiation balance for different underlying surfaces. To simulate radiation balance differences, we set four pure land-cover types (forest, grass, roads, and buildings). Keeping all other conditions inputted unchanged, we model the radiation balance by changing the land-cover type. The results show that the effects of different underlying surfaces on radiation differ, and that there is much upward long-wave radiation, accounting for 84.3% of the total radiation energy falling incident on the land surface. The annual averages of net radiation for the four land-cover types are in the range of 38.2–53.4 W/m^2. The net radiation of the grass surface is minimal while that of the roads surface is maximal. Additionally, with urbanization the net radiation values of common types of land-cover change, such as conversion from forest to roads, grass to roads, and grass to buildings, all have increasing trends, indicating that net radiation usually increases with urban sprawl.

net all-wave radiation parameterization, net radiation, urban heat island, energy balance, climate change, Beijing

Citation: Cui Y P, Liu J Y, Hu Y F, et al. Modeling the radiation balance of different urban underlying surfaces. Chin Sci Bull, 2012, 57: 1046–1054, doi: 10.1007/s11434- 011-4933-x

Land surfaces interact with the atmosphere through the exchange of water, energy and momentum. Any changes in energy flux between the land and atmosphere will affect the atmospheric thermal conditions and atmospheric circulation. The underlying surfaces (land use/land cover classes) greatly affect the climate according to their physical properties, such as the surface albedo, roughness, and emissivity [1]. The components of the radiation balance, the net radiation in particular, are main components of the land surface energy budget and are important physical and ecological parameters in the land-atmosphere energy exchange and redistribution [2].

The relationship between the type of urban underlying surface and the radiation energy budget is a core issue of urban climate. The effect of the urban land surface energy flux on local climate has been verified in many studies [3]. Therefore, systematic analysis of the urban radiation balance of various underlying surfaces is a basis and prerequisite for urban energy balance studies, and it is also important in understanding change processes of urban energy for different underlying surfaces and local climate caused by urban sprawl [4].

The basic characteristic of urban landscape is the spatial heterogeneity of its land surfaces, and differences in landscape composition lead to the nonuniformity of energy transmission and distribution. Urban land surface is a complex physical interface. As surface characteristics change, the thermodynamic and kinetic properties of underlying surfaces can substantially change. All these disturbance factors will result in city-specific climatic characteristics. Most previous studies in this area of research have analyzed urban-rural radiation differences using climatic models,

*Corresponding author (email: kuangwh@lreis.ac.cn)

terrestrial ecosystem models, or computational fluid dynamics models. However, as all these studies combined the radiation differences of landscape heterogeneity, it was difficult for them to explain the energy transformation processes of different underlying surfaces [5], and local micro-climate characteristics within a city were not accurately simulated [6]. In addition, owing to the variety of influencing factors, the observations of meteorological stations cannot effectively distinguish the effects of underlying surfaces on radiation balance components, and there are even conflicting observation results. For example, according to observations made in St. Louis, White et al. [7] found that the net radiation in the city was less than that in the suburbs in summer (by 4%); the Basel Urban Boundary Layer Experiment (BUBBLE) observed that urban net radiation was slightly less than suburban net radiation, and found that it was necessary to analyze the radiation differences of underlying surfaces in urban and rural areas [8]; and Peng et al. [9] showed that urban net radiation was much greater than suburban net radiation. Therefore, to clarify the effects of the underlying surface on the radiation balance, it is necessary to use limited parameters by considering pure underlying surfaces to analyze the change processes of the land surface radiation budget.

The objective of this study is to demonstrate the corresponding relationship between the radiation energy flux and the underlying surface. A relatively new urban surface radiation parameterization scheme [10] (net all-wave radiation parameterization, NARP) is applied to simulate the radiation change processes of each underlying surface and then analyze the radiation changes corresponding to conversion of the underlying surface.

1 Data source and methodology

1.1 Research data

Meteorology and radiation data were collected by the Beijing urban ecosystem research station of the Chinese Ecosystem Research Network. The observation equipment was installed on the roof of a building of the Research Center for Eco-Environmental Sciences, Chinese Academy of Sciences, between the North Fourth Ring Road and Fifth Ring Road in Beijing. The observation station is a typical city office in a residential area (more than 70% of the surface is impervious surface). We compared the station data with another site data during the same time period and found that the observation data are continuous and stable. The observed indicators were routine meteorological and radiation indicators (temperature, pressure, precipitation, relative humidity, wind speed, wind direction, downward short-wave radiation and net radiation). In this study, the data used were observations for the year 2010 with a time interval of 10 minutes.

This study first tested the accuracy of NARP and then carried out simulation experiments. We artificially set four pure underlying surfaces, namely forest, grass, roads and buildings. Keeping other conditions unchanged, the radiation balance for different underlying surfaces and their conversion were simulated by NARP.

1.2 NARP scheme

Net radiation (R_n) and its components can be expressed as

$$R_n = K^* + L^* = K_\downarrow - K_\uparrow + L_\downarrow - L_\uparrow , \quad (1)$$

where K and L are the short-wave radiation and long-wave radiation fluxes, respectively; * denotes the net radiation flux; and arrows indicate the direction of the radiation flux. In the following text, we denote the net radiation, upward short-wave radiation, downward short-wave radiation, upward long-wave radiation, and downward long-wave radiation by *qn*, *ku*, *kd*, *lu*, and *ld*, respectively.

(i) Net short-wave radiation. Net short-wave radiation is expressed as

$$K^* = K_\downarrow \left(1-\alpha_0\right), \quad (2)$$

where α_0 is the surface albedo, which is set in this study according to previous studies (Table 1). Albedo is a function of the sun elevation angle and land surface properties. Its diurnal variation can be expressed as

$$\alpha_0(\psi) = \alpha + (1-\alpha)\exp\left[-0.1\psi - (1-\alpha)/2\right], \quad (3)$$

where α is the maximum albedo when the sun elevation angle (ψ, degrees) reaches a maximum [11]. Albedo can also be accurately obtained from the observed net radiation, downward short-wave radiation and long-wave radiation:

$$\alpha_{0,d} = \left(K_\downarrow + L_\downarrow - L_\uparrow - R_n\right)\big/K_\downarrow . \quad (4)$$

(ii) Downward long-wave radiation (*ld*). NARP provides two methods to simulate the urban radiation balance. The first method is to use a single-layer atmospheric model:

$$L_\downarrow = \varepsilon_{sky}\sigma T_{sky}^4 , \quad (5)$$

where T_{sky} is the bulk atmospheric temperature (K), which can be estimated approximately from the near-surface temperature; σ is Stefan's constant; and ε_{sky} is the broadband atmospheric emissivity, which can be separately estimated in clear-sky or cloudy cases. In clear-sky situations, the expression is [12]

$$\varepsilon_{clear} = 1-(1+w)\exp\left[-(1.2+3.0w)^{0.5}\right], \quad (6)$$

where w is the precipitable water content (g/cm^2) approximated by mean atmospheric values of vapor pressure (e_a) and temperature (T_a) at the reference height in the surface layer:

$$w = 46.5e_a/T_a . \quad (7)$$

In the case of a cloudy day,

$$K_{\downarrow,\mathrm{clear}} = I_{\odot}\cos(z)\tau_{\mathrm{R}}\tau_{\mathrm{pg}}\tau_{\mathrm{w}}\tau_{\mathrm{aer}}, \tag{8}$$

where $I_{\odot}$ is extraterrestrial solar insolation, z is the solar zenith angle, and $\tau_{\mathrm{R}}\tau_{\mathrm{pg}}\tau_{\mathrm{w}}\tau_{\mathrm{aer}}$ is the product of transmissivities for Rayleigh scattering (R), absorption by permanent gases (pg) and water vapor (w), and absorption and scattering by aerosols (aer), which are functions of the time of year, zenith angle, latitude, surface dew point (computed from observed T_{a} and relative humidity), and surface pressure.

The daytime cloud fraction (F_{CLD}) is calculated as

$$F_{\mathrm{CLD}} = 1 - K_{\downarrow}/K_{\downarrow,\mathrm{clear}}, \tag{9}$$

here the computing deviation of cloud fraction can be minimized by taking the square [12]:

$$\varepsilon_{\mathrm{sky}} = \varepsilon_{\mathrm{clear}} + (1-\varepsilon_{\mathrm{clear}})F_{\mathrm{CLD}}^2. \tag{10}$$

The approach has some bias when the zenith angle is greater than 80° (the cosine response) [13]. Therefore, a new expression is considered:

$$F_{\mathrm{CLD}} = 0.185\left(\mathrm{e}^{(0.015+1.9\times10^{-4}T_{\mathrm{a}})*RH} - 1\right), \tag{11}$$

$$L_{\downarrow} = \left[\varepsilon_{\mathrm{clear}} + \left(1-\varepsilon_{\mathrm{clear}}\right)* F_{\mathrm{CLD}}\right]*\sigma T_{\mathrm{a}}^4. \tag{12}$$

According to Loridan and Grimoond, the simulative accuracy of *ld* improves with the root mean square error (RMSE) dropping from 33.3 to 31.6 W/m^2 and the mean bias error (MBE) reducing from −15.3 to 2.9 W/m^2. In this study, the improved method is used to calculate *ld* [14].

(iii) Upward long-wave radiation (*lu*). Upward long-wave radiation is given by

$$L_{\uparrow} = \varepsilon_0\sigma T_0^4 + \left(1-\varepsilon_0\right)L_{\downarrow}, \tag{13}$$

lu is mainly dependent on the surface temperature (T_0) and emissivity. As T_0 is difficult to observe over a large spatial region, T_0 here is estimated by T_0 following previous studies [10,15,16]. Because the air temperature and surface temperature during the day (night) are quite different, *kd* is used to correct the diurnal surface temperature. The expression is

$$\begin{aligned}\varepsilon_0\sigma T_0^4 &\approx \varepsilon_0\sigma T_{\mathrm{a}}^4 + 4\varepsilon_0\sigma T_{\mathrm{a}}^3(T_0 - T_a)\\ &= \varepsilon_0\sigma T_{\mathrm{a}}^4 + cK_{\downarrow}(1-\alpha_0),\end{aligned} \tag{14}$$

where $c = 0.08$ [10,15]. Therefore, *lu* can be expressed as

$$L_{\uparrow} = \varepsilon_0\sigma T_{\mathrm{a}}^4 + 0.08K_{\downarrow}\left(1-\alpha_0\right) + \left(1-\varepsilon_0\right)L_{\downarrow}. \tag{15}$$

Although it is difficult to make the nighttime correction, the effect of the nighttime correction on the overall accuracy is limited. This is especially true for urban centers. There are two main reasons for using the estimated T_0. On one hand, the current precision level of the infrared radiometer is lower than 0.5°C, while the technology of air temperature observations is mature and has relatively high accuracy. On the other hand, the estimated T_0 meets the simulation needs [17], having an RMSE of 4.9–12.9 W/m^2. Moreover, the lack of a nocturnal correction may be more acceptable in urban areas [10]. This is because the nocturnal release of stored heat from the urban fabric is sufficient to produce upward-directed convective sensible heat flux [18], and the air tends to be neutral [19]. Grimmond's comparison test also confirmed that the simulated upward long-wave radiation had higher accuracy at night; the RMSE was 20 W/m^2 during the daytime but dropped to about 10 W/m^2 at night [20].

The net radiation and four radiation components can thus be calculated. Among them, as an important parameter, *kd* is inputted as observation data. Albedo and emissivity greatly affect the results. Owing to the lack of measurement data for Beijing, we have mainly referenced others' results in setting values [21,22]. The parameters used are given in Table 1.

1.3 Accuracy test methods

In this study, four kinds of statistical indices, namely the correlation coefficient (r), RMSE (W/m^2), mean bias error (MBE, W/m^2), and simulation efficiency (EF), are employed to test model accuracy. They can be respectively expressed as

$$r_{x,y} = \frac{\sum_{i=1}^{n}(x_i-\overline{x})(y_i-\overline{y})}{\sqrt{\sum_{i=1}^{n}(x_i-\overline{x})^2}\sqrt{\sum_{i=1}^{n}(y_i-\overline{y})^2}}, \tag{16}$$

$$\mathrm{RMSE} = \sqrt{\frac{1}{n}\sum_{i=1}^{n}(x_i-y_i)^2}, \tag{17}$$

$$\mathrm{MBE} = \frac{1}{n}\sum_{i=1}^{n}(x_i-y_i), \tag{18}$$

$$\mathrm{EF} = 1 - \left[\sum_{i=1}^{n}(x_i-y_i)^2 \Big/ \sum_{i=1}^{n}(y_i-\overline{y})^2\right], \tag{19}$$

where x is the simulated value, y is the observed value, and n is the sample number. r indicates the linear correlation between the observed values and the simulated values. RMSE evaluates the consistency between the simulated

Table 1 Corresponding parameters of different urban underlying surfaces

Underlying surfaces	Albedo	Reference	Emissivity	Reference
Roads	0.125	[21]	0.95	[21]
Buildings	0.224	[21,22]	0.91	[21]
Forest	0.18	[21]	0.975	[21]
Grass	0.25	[21,22]	0.93	[21]

values and the observed values. MBE reflects the average deviation between the simulated values and the observed values, with a positive value indicating an overestimating trend and a negative value indicating an underestimating trend, and the best MBE value thus being zero. EF is the consistency proportion of the simulated values to the observed values, with higher EF indicating better simulation accuracy.

2 Results and analysis

2.1 NARP accuracy analysis

NARP has been effectively verified for several cities [10,18,23]. To analyze the parameterization scheme's reliability in the case of Beijing, this study tests its accuracy with station data for the whole year of 2010. Figure 1(a) shows the relationship between the simulated values and the observed values. It is seen that almost all values appear near the 1∶1 dotted line, with the best fit having a slope of 0.95 and a fitting coefficient (R^2) of 0.95. To visualize the daily matching of simulated and observed values, the daily changes of random 150–250 days of the year are presented (Figure 1(b)), and the result shows that the observed net radiation and the simulated net radiation are consistent.

From the statistical results, we find that the correlation coefficient r is greater than 0.9 and passes the significance test (Table 2). Meanwhile, the monthly average RMSE is less than 30.0 W/m^2. MBE indicates that the net radiation is underestimated by NARP except in June. The absolute maxima of the monthly average MBE appear in March and February, and the absolute values are all greater than 20.0 W/m^2. EF shows that the simulation efficiency is less than 90% in winter (December, January, and February). A possible reason may be the daily variation parameters (albedo and emissivity) are instead by fixed values in NARP. However, the annual average EF exceeds 90%, especially in the vegetation growing season. In summary, NARP simulates the net radiation well in most of the year, and can thus be used to analyze the radiation balance of Beijing.

2.2 Radiation balance differences of underlying surfaces

This study analyzes the effects of four pure underlying surfaces (forest, grass, roads, and buildings) on the radiation balance. Because *kd* is observation data, *ld* is calculated from the same relative humidity, temperature and other station data (eqs. (5) and (12)), and the radiation differences of different underlying surfaces are thus mainly the differences in *qn*, *ku*, and *lu*.

Figure 2(a) clearly shows the *qn* differences for different underlying surfaces (the dashed line is the 1∶1 reference line of forest net radiation). The slope expresses the size of the radiation flux, the order of which is roads > forest > buildings > grass. Figure 2(b) presents the monthly changes in *qn* for the four underlying surfaces. It is seen that the maximum values of net radiation appear in June and the minimum values appear in December. The maximum values

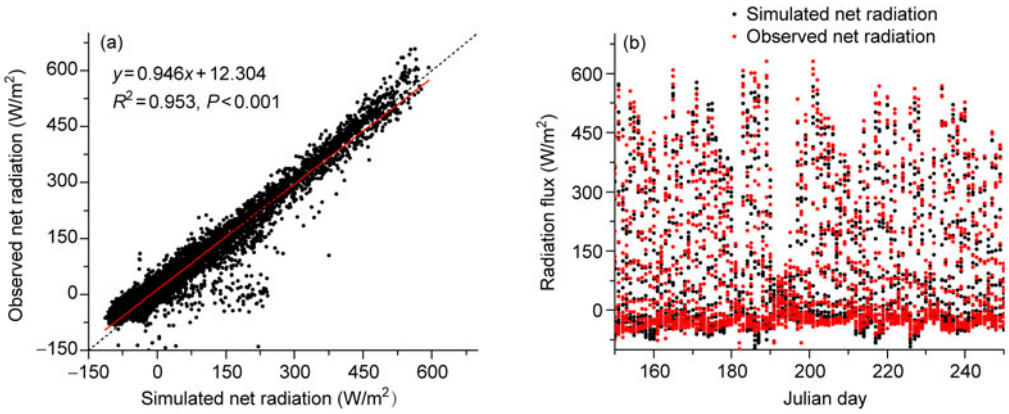

Figure 1 Scatter plot of simulated and observed net radiation.

Table 2 Statistical comparisons of observed and simulated net radiation

	Jan	Feb	Mar	Apr	May	Jun	Jul	Aug	Sept	Oct	Nov	Dec	Mean
r	0.97	0.96	0.97	0.99	0.99	0.99	0.99	0.99	0.99	0.99	0.98	0.97	0.98
RMSE (W/m^2)	34.67	37.74	43.23	29.56	31.98	21.85	25.71	29.24	18.19	24.23	27.10	33.52	29.75
MBE (W/m^2)	−14.77	−23.98	−25.58	−14.79	−17.88	0.54	−4.29	−0.51	−0.14	−11.86	−10.60	−12.04	−11.33
EF	0.86	0.82	0.92	0.98	0.98	0.99	0.98	0.98	0.99	0.97	0.92	0.78	0.93

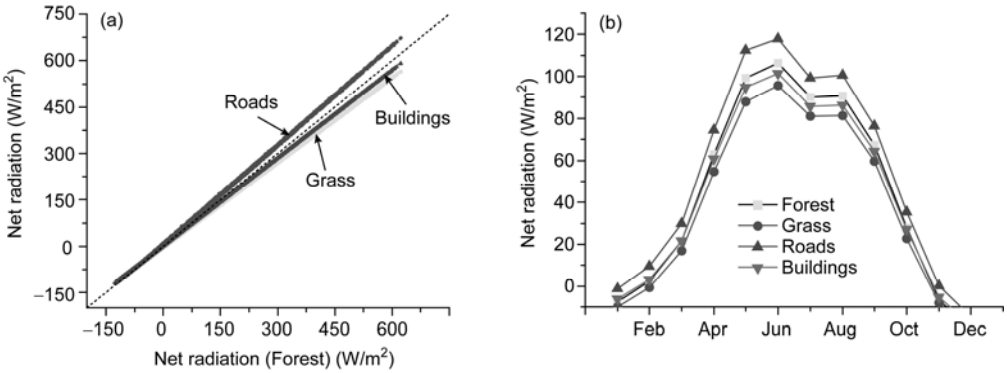

Figure 2 Net radiation differences for different underlying surfaces.

of *qn* are 117.8 W/m^2 for roads, 106.4 W/m^2 for forest, 101.3 W/m^2 for buildings, and 95.5 W/m^2 for grass. The *qn* sequences of different underlying surfaces are the same as in the results of Figure 2(a). We also find the net radiation difference between forest and buildings decreases in winter.

The scatter plot of *ku* shows the change trends of different underlying surfaces (Figure 3(a)). *ku* for buildings is less than that for grass, but it is still much larger than that for forest. Roads have the minimum *ku*, with an annual mean value of 18.0 W/m^2. Figure 3(b) shows the overall *ku* is in the range of 10.0–60.0 W/m^2. The maximum *ku* values for the four underlying surfaces are all in May. Specifically, the maximum values are 56.73 W/m^2 for grass, 40.85 W/m^2 for forest, 28.37 W/m^2 for roads, and 50.81 W/m^2 for buildings. These results mainly reflect the effect of surface albedo.

lu has a large effect on net radiation, especially at night. Overall, the values of *lu* for the four underlying surfaces are all small (Figure 4(b)). To better indicate the differences of the four underlying surfaces, Figure 4(a) is an enlarged scatter plot for one period of the year 2010. It shows that roads and forest have higher *lu* values, while buildings and grass have lower *lu* values and they are hard to separate. The monthly fluctuation range is between 300.0 and 480.0 W/m^2, with the minimum appearing in January and the maximum

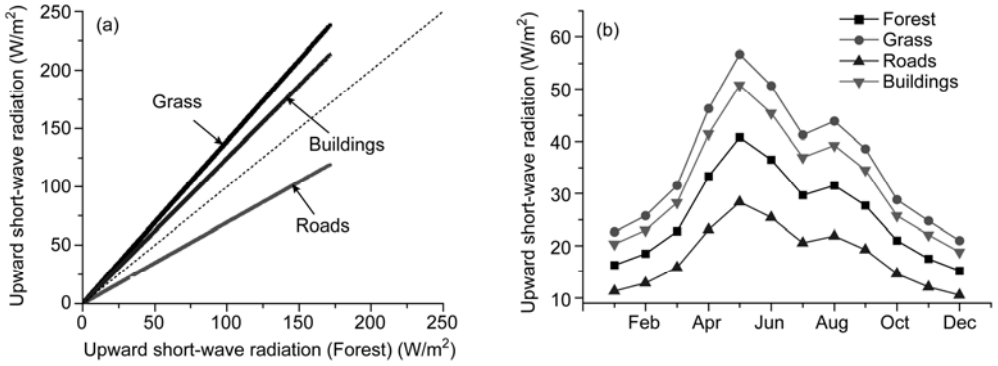

Figure 3 Upward short-wave radiation differences for different underlying surfaces.

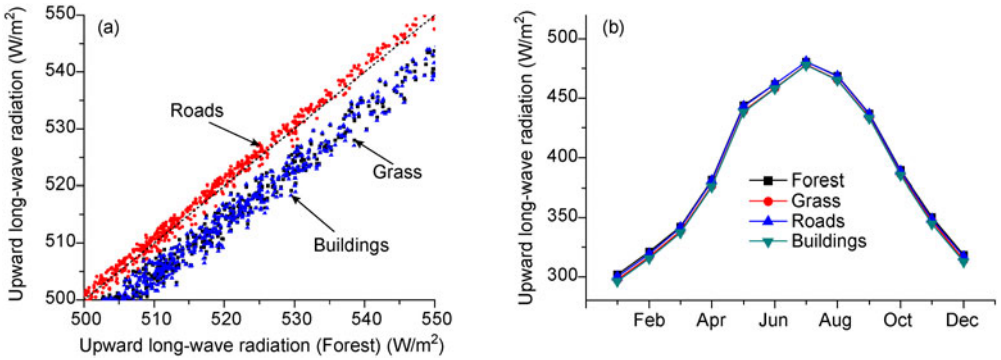

Figure 4 Upward long-wave radiation differences of different underlying surfaces.

in July. These results are also consistent with the observed value for a forest area reported by Wang et al. [24]. According to Kirchhoff's law and the Stefan-Boltzmann law, the surface emissivity and especially the surface temperature affect *lu*. The air temperature near land surface directly affects the surface temperature, and therefore, its variation corresponds well to temperature changes throughout the year.

Table 3 presents the upward and downward (including short-wave and long-wave) radiation flux ratios of the four underlying surfaces. Simulation results show that seasonal variations in ratio of the four underlying surfaces have the same trend and the ratio differences are all small (less than 0.02). The ratios are highest in summer followed by spring, autumn, and winter. The upward radiation fluxes of common urban land coverage types such as buildings and roads are slightly higher than those of grass and forest. However, given that grass and forest also cover quite a large portion of urban areas, the role of the ratio difference is limited in analyzing the urban radiation balance.

The descending order of the five radiation components is *lu*>*ld*>*kd*>*qn*>*ku*. The annual average of *lu* is 386.7–391.4 W/m^2, while the annual average of *ku* and *qn* are in the range of 18.0–36.0 W/m^2 and 38.2–53.4 W/m^2, respectively. The sum of *qn* for buildings and roads is larger than that for forests and grass. However, it should be noted that there are still significant radiation differences among vegetation cover types such as forest and grass, or man-made types such as buildings and roads. While the upward/downward ratio differences are small between the two vegetation coverage types and the two man-made coverage types, even the ratio of grass is less than that of buildings during the vegetation growing season. Comparing with other studies shows that there are certain controversies in the result [9], indicating that more studies are needed. Even so, if only using the upward radiation fluxes to analyze the energy issue, the effect of the vegetation coverage area on regulation of the urban energy budget would be underestimated. This is because vegetation generates much latent heat in the growing season, which has a decisive effect on energy redistribution.

In fact, here *ku* and *lu* together affect the net radiation. *ku* is mainly affected by surface albedo, and its annual average *ku* for the four underlying surfaces is 28.7 W/m^2. *lu* is mainly affected by the emissivity and surface temperature, and its annual average for the four underlying surfaces is 389.1 W/m^2, accounting for 84.3% of the total incoming solar radiation, indicating its important role in the radiation balance.

Table 3 Upward and downward radiation flux ratios for the four types of underlying surfaces

$(K_\uparrow + L_\uparrow)/(K_\downarrow + L_\downarrow)$	Spring	Summer	Autumn	Winter	Mean
Forest	0.89	1.03	0.87	0.71	0.88
Grass	0.90	1.11	0.90	0.72	0.91
Roads	0.89	1.07	0.88	0.70	0.89
Buildings	0.92	1.10	0.90	0.71	0.91

2.3 Net radiation differences of underlying surfaces changes

The differences of underlying surfaces directly result in the differences in radiation balance components. There are always changes in land use/land cover with urbanization. Additionally, the land use/land cover change will ultimately affect the urban solar energy income, namely the net radiation. Here we analyze changes in net radiation resulting from underlying surface conversions one by one. Figure 5 shows the changes in radiation components for six conversions of underlying surfaces: forest to grass, forest to roads, forest to buildings, grass to roads, grass to buildings, and roads to buildings. When the conversion is in the opposite direction, the ± signs of the corresponding values are reversed accordingly.

Figure 5(a) shows the monthly radiation difference for conversion from forest to grass. We find that net radiation decreases (forest – grass > 0), and the decrease even exceeds 10.0 W/m^2 in some months. In addition, *ku* increases and *lu* decreases. Figure 5(b) presents the radiation difference for conversion from forest to roads. It is seen that *qn* has a remarkable increasing trend, and it reaches a maximum in May. Meanwhile, *ku* and *lu* decrease over the year. Figure 5(c) shows the radiation difference for conversion from forest to buildings. Overall, *qn* experiences a downward trend from March to November, namely the vegetation growing season, but it briefly increases in winter. Meanwhile, *lu* and *ku* increase throughout the year. Figure 5(d) presents the radiation difference for conversion from grass to roads. The net radiation has a greater increasing trend than that for conversion from forest to roads, reaching a maximum of 25.0 W/m^2 in May. *ku* has a decreasing trend similar to that for conversion from forest to roads, while *lu* has a slight increasing trend. Figure 5(e) presents the radiation difference for conversion from grass to buildings. It is seen that, although the radiation change is small and within a range of ±8.0 W/m^2, there is a clear change law. The net radiation difference for conversion from grass to roads has an increasing trend, while *ku* and *lu* have decreasing trends. Roads and buildings are typical man-made land surfaces in urban areas. However, owing to the intrinsic differences of materials, the effects of roads and buildings on each radiation component differ (Figure 5(f)). The change in *qn* for conversion from roads to buildings decreases and reaches its maximum of close to 20.0 W/m^2 in May. Meanwhile, *ku* increases and *lu* decreases slightly.

To better understand the net radiation changes of different types of underlying surface conversion, the conversion matrix of the annual average *qn* is presented in Table 4. It shows that *qn* increases during conversion from forest to roads, grass to forest, grass to roads, grass to buildings, and

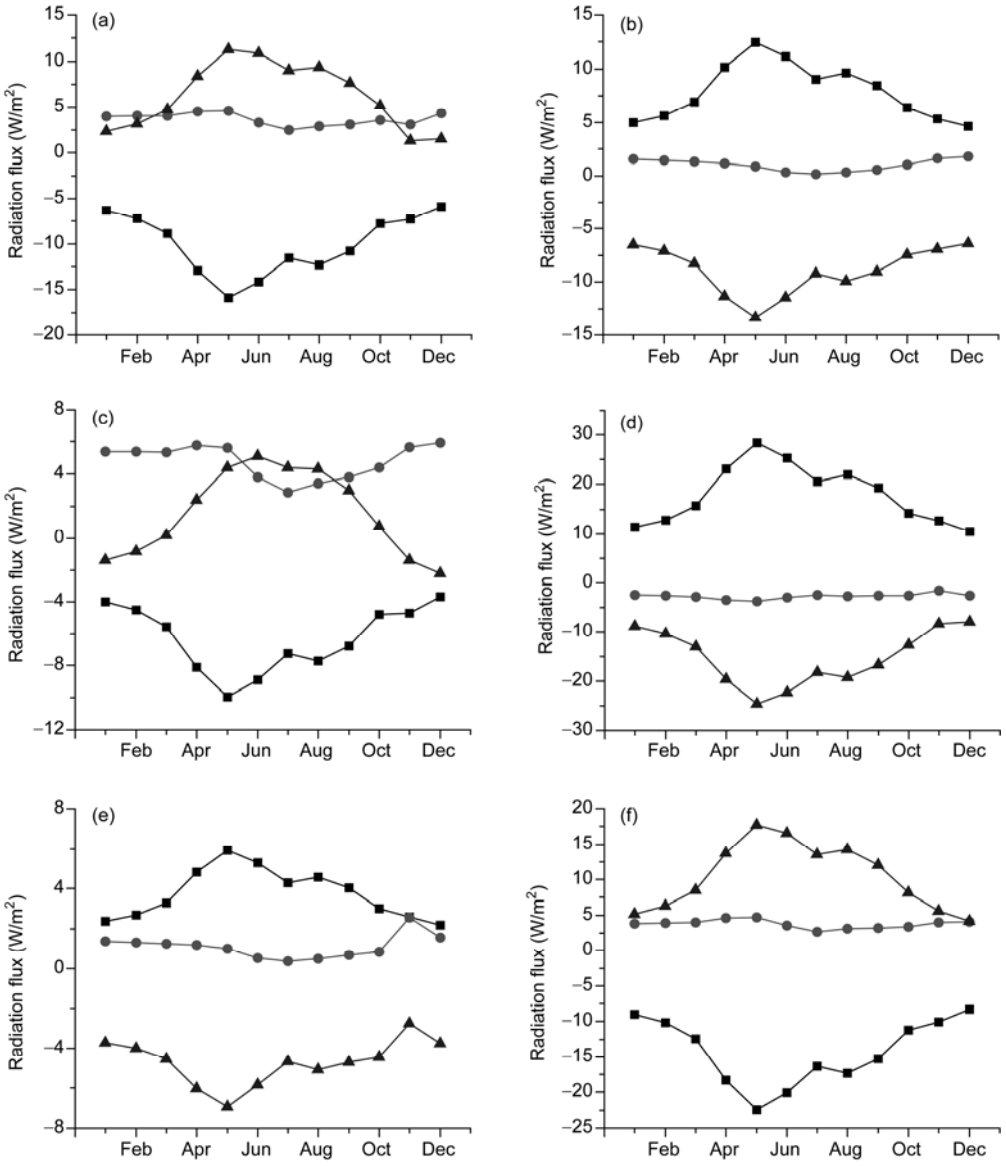

Figure 5 Net radiation differences for conversions of underlying surfaces. (a) Forest to grass; (b) forest to roads; (c) forest to buildings; (d) grass to roads; (e) grass to buildings; (f) roads to buildings. —■—, Upward short-wave radiation; —●—, upward long-wave radiation; —▲—, net radiation.

Table 4 Annual average changes in net radiation for different conversion types

	Forest	Grass	Roads	Buildings
Forest	–	–6.24	8.92	–1.54
Grass	6.24	–	15.16	4.70
Roads	–8.92	–15.16	–	–10.46
Buildings	1.54	–4.70	10.46	–

buildings to forest, while net radiation decreases for the other four conversion types. Among them, *qn* has a significant increasing trend when grass is converted to roads, while it has only a slight change when forest is converted to buildings, with an annual change of –1.54 W/m^2.

In summary, when there is conversion from forest to roads, grass to roads, and grass to buildings, the net radiation increases, and the change maxima are 13.33, 24.62 and 6.92 W/m^2, respectively. In fact, these three underlying surfaces conversion types are all associated with urban sprawl. For a city, urbanization means that farmland, grass and forest disappear and roads and buildings account for more land area year by year; therefore, in terms of underlying surfaces, urban net radiation has an increasing trend. The results also are consistent with the conclusions of Oke et al. [25]. It must be pointed out that conversion from forest to buildings is a special case, having a decreasing trend in the vegetation growing season but an increasing trend in winter. The net radiation increases in conversions from forest to grass and roads to buildings, which may explain why some studies found that rural net radiation was slight greater than urban

net radiation (0.1 W/m^2) [8]. In addition, the net radiation differences fluctuate significantly in the vegetation growing season, implying that changes in solar zenith angle, vegetation and other factors remarkably affect the urban radiation balance.

3 Discussion and conclusions

3.1 NARP limitations

Net radiation, as an important land-atmosphere energy exchange parameter, can be obtained by employing three methods. The first is direct observation; the second is model simulation, including climate models; and the third is fitting with other radiation components. However, quite a few net radiation parameterization schemes can be used to accurately estimate the urban radiation balance [10]. The RMSE of current models is between 22.1 and 92.3 W/m^2, and MEB values are –40.6 to 62.4 W/m^2. Many models perform well in summer or at night, but poorly in winter or during the day. It is worth noting that the net radiation obtained by the ordinary least squares regression model based on downward short-wave radiation can produce better results, even achieving an RMSE of less than 30 W/m^2 in some urban areas [20,23,26].

NARP was mainly proposed and developed by Holtslag and Crawford to simulate the radiation budget in non-urban natural areas [15,27]. The radiation balance is affected by the spatial scale. Offerle et al. improved the scheme so that it can be used in urban areas [10,14]. As NARP is a flat model, the radiation-shielding effect of buildings and multiple-reflection absorption are not considered in the model, and it is thus only suitable for application on a local urban scale. Niemelä et al. [28] studied the simulation accuracies for urban net radiation of different parameters schemes, finding that under the limit of clear-sky conditions, the RMSE values of general schemes were 12–49 W/m^2 and those of complex schemes were 11–19 W/m^2. In this study, NARP has already achieved high precision, with RMSE 29.75 W/m^2, MBE –11.33 W/m^2, and EF 0.93 under various weather conditions of the year 2010. However, the NARP algorithm, albedo, and space scale expansion problems still need to be addressed in the future.

Albedo greatly affects simulation results but is difficult to determine. This study set constants corresponding to each underlying surface. One question is whether an appointed albedo value can replace the real varying albedo. According to the findings of Sailor and Fan, a typical albedo value may be better than a dynamic albedo [29]. Offerle et al. [10] found that the diurnal variation albedo had little effect on net radiation and that it did not significantly improve the model accuracy (RMSE dropped by only 0.6 W/m^2). The simulation results of more than 20 models also showed that, comparing with the use of multiple albedo values, the use of a fixed albedo had minimal effect on the accuracy of short-wave radiation, and the use of a single underlying surface may produce the least error. Meanwhile, some previous studies showed that the simulation accuracy of NARP could be greatly improved with a precise albedo having diurnal variation, with the RMSE dropping by 23.8 W/m^2 and MBE dropping by 24.9 W/m^2 [10]. We believe that it should be possible to improve the simulation accuracy when considering the dynamical albedo of underlying surfaces, but that a relatively accurate and representative albedo should be available.

3.2 Conclusions

The core issue of urban land-atmosphere energy research is to objectively describe the main physical process, namely the radiation and energy balance process. In this study, meteorological observation data for 2010 are used to verify NARP. We then set four typical urban underlying surfaces (forest, grass, roads, and buildings) to simulate the urban radiation balance using the tested NARP. The main conclusions of this study are as follows:

(1) As a general urban net radiation parameterization scheme, NARP can be used to simulate the radiation balance of Beijing, with annual simulation efficiency reaching 0.93.

(2) Radiation components significantly differ depending on the underlying surface. The annual averages of net radiation for roads, forest, buildings, and grass are 53.4, 44.4, 42.9, and 38.2 W/m^2, respectively.

(3) The analysis of underlying surface conversions shows that net radiation continues to increase when there are common conversion types of urban sprawl, such as conversion from forest to roads, grass to roads, and grass to buildings. Meanwhile, the net radiation decreases during conversion from forest to buildings, forest to grass, and roads to buildings. Therefore, we should analyze the effects of urban sprawl on the radiation balance according to specific conversions of underlying surfaces.

This work was supported by the National Basic Research Program of China (2010CB950902), the National Natural Science Foundation of China (40971223 and 40901224), and the Major Program for the Fundamental Research of the Chinese Academy of Sciences (KZCX2-EW-306). The authors thank Profs. Grimmond C S B, Wang Xiaoke and Dr. Ren Yufen for providing invaluable support.

1 Yin Y H, Wu S H, Dai E F. Determining factors in potential evapotranspiration changes over China in the period 1971–2008. Chin Sci Bull, 2010, 55: 3329–3337
2 Dabberdt W F, Lenschow D H, Horst T W, et al. Atmosphere-surface exchange measurements. Science, 1993, 260: 1472–1481
3 Arnfield A J. Two decades of urban climate research: A review of turbulence, exchanges of energy and water, and the urban heat island. Int J Climatol, 2003, 23: 1–26
4 Wang X Q, Gong Y B. The impact of an urban dry island on the summer heat wave and sultry weather in Beijing City. Chin Sci Bull, 2010, 55: 1657–1661

5 Zhang H Y, Rao S, Chi Y Y, et al. Advances in the impacts of urban landscape pattern on urban air environment (in Chinese). Adv Earth Sci, 2006, 21: 1025–1032
6 Tong H, Chan J C L, Sang J G. A study of the urban boundary layer model and its applicatin in the Hong Kong area (in Chinese). Chin J Atmos Sci, 2004, 28: 957–978
7 White J M, Eaton F D, Auer A H. The net radiation budget of the St. Louis metropolitan area. J Appl Meteorol, 1978, 17: 593–599
8 Christen A, Vogt R. Energy and radiation balance of a central European city. Int J Climatol, 2004, 24: 1395–1421
9 Peng J L, Wu X, Jiang Z H, et al. Characteristics analysis of energ budget over urban and suburban underlying surfaces in Nanjing (in Chinese). Sci Meteorol Sin, 2008, 28: 21–29
10 Offerle B, Grimmond C S B, Oke T R. Parameterization of net all-wave radiation for urban areas. J Appl Meteorol, 2003, 42: 1157–1173
11 U.S. Environmental Proection Agency. Pcrammet User's Guide, Technical Report. In: U.S. Environmental Proection Agency, Office of Air Quality Planning and Standards, Emissions, Monitoring, and Analysis Division. 1999. 95
12 Prata A. A new long-wave formula for estimating downward clear-sky radiation at the surface. Q J Roy Meteor Soc, 1996, 122: 1127–1151
13 Batlles F J, Olmo F J, Tovar J, et al. Comparison of cloudless sky parameterizations of solar irradianceat various spanish midlatitude Locations. Theor Appl Climatol, 2000, 66: 81–93
14 Loridan T, Grimoond C S B, Offerle B D, et al. Local-scale urban meteorological parameterization scheme (LUMPS): Longwave radiation parameterization and seasonality-related developments. J Appl Meteorol Climatol, 2011, 50: 185–202
15 Holtslag A A M, van Ulden A P. A simple scheme for daytime estimates of the surface fluxes from routine weather data. J Appl Meteorol, 1983, 22: 517–529
16 van Ulden A P, Holtslag A A M. Estimation of atmospheric boundary layer parameters for diffusion applications. J Clim Appl Meteorol, 1985, 24: 1196–1207
17 de Rooy W, Holtslag A A M. Estimation of surface radiation and energy flux densities from single-level weather data. J Appl Meteorol, 1999, 38: 526–540
18 Grimmond C S B, Oke T R. Turbulent heat fluxes in urban areas: Observations and a local-scale urban meteorological parameterization scheme (LUMPS). J Appl Meteorol, 2002, 41: 792–810
19 Oke T R. The heat island of the urban boundary layer: Characteristics, causes and effects. In: Cermak J E, Davenport A G, Plate E J, et al., eds. Wind Climate in Cities. Waldbronn: Kluwer Academic Publishers, 1995. 81–107
20 Grimmond C, Blackett M, Best M, et al. Initial results from Phase 2 of the international urban energy balance comparison project. Int J Climatol, 2011, 31: 244–272
21 Oke T R. Boundary Layer Climate. London: Routledge Press, 1987
22 Zhou S Z, Shu T. Urban Climatology (in Chinese). Beijing: Chinese Meteorological Press, 1994. 156
23 Grimmond C S B, Blackett M, Best M J, et al. The international urban energy balance models comparison project: First results from phase 1. J Appl Meteorol Climatol, 2010, 49: 1268–1292
24 Wang X, Zhou G Y, Sun G, et al. Characteristic of radiation flux of coniferous and broadleaved mixed forest in low subtropical China (in Chinese). J Beijing Forestry Univ, 2006, 28: 28–34
25 Oke T R, Shen J Z (translator). A review on water, radiation, and energy balance in urban climate (in Chinese). Prog Geogr, 1983, 2: 25–30
26 Badescu V. Verification of some very simple clear and cloudy sky models to evaluate global solar irradiance. Sol Energy, 1998, 61: 251–264
27 Crawford T M, Duchon C E. An improved parameterization for estimating effective atmospheric emissivity for use in calculating daytime down-welling, long-wave radiation. J Appl Meteorol, 1999, 38: 474–480
28 Niemelä S, Räisänen P, Savijärvi H. Comparison of surface radiative flux parameterizations: Part II. Shortwave radiation. Atmos Res, 2001, 58: 141–154
29 Sailor D J, Fan H. Modeling the diurnal variability of effective albedo for cities. Atmos Environ, 2002, 36: 713–725